INTERNATIONAL JOURNAL OF FLUID POWER, 2017
VOL. 18, NO. 1, 38–48
http://dx.doi.org/10.1080/14399776.2016.1213115

Taylor & Francis
Taylor & Francis Group

A temperature adaptive piston design for swash plate type axial piston machines

Lizhi Shang and Monika Ivantysynova

Department of Agricultural and Biological Engineering, Purdue University, West Lafayette, IN, USA

ABSTRACT

The authors propose a temperature adaptive piston design for axial piston machines of swash plate type. The proposed piston helps to keep the film thickness between piston and cylinder close to optimal with respect to energy dissipation while operating temperature can change in a wide range. The authors utilize the thermal deformation of piston and cylinder, which varies with temperature, to design the interface that adapt the gap height to compensate the change of the fluid viscosity with the temperature. An in-house developed fluid-structure and thermal interaction model together with recently developed port and case temperature prediction model are used to analyze the piston/cylinder interface and to predict resulting part temperatures, deformations, the fluid film properties and resulting energy dissipation, friction and leakage of the proposed novel design. The results show a reduction of energy dissipation over a large range of operating temperature for the proposed design compared to the baseline design.

ARTICLE HISTORY
Received 29 March 2016
Accepted 12 July 2016

KEYWORDS
Axial piston machine; piston/cylinder interface; thermal deformation; energy dissipation in fluid film

1. Introduction

The piston/cylinder interface in swash plate type axial piston machines is the most complicated tribological interface in terms of balancing high pressure forces. The piston cannot be hydrostatically balanced like the slipper/swash plate or slipper/outer ring and the cylinder block/valve plate interface, which can be designed as combined hydrostatic/hydrodynamic bearing. The successful design of the piston/cylinder interface determines the achievable maximum operating pressure, maximum speed and maximum swash plate angle of an axial piston machine. A very challenging design goal is to avoid wear by creating a sufficient load carrying ability of the fluid film and to minimize energy dissipation in a wide range of operating conditions in order to achieve a very high machine efficiency. The piston/cylinder interface represents a very complex hydrodynamic bearing, which has to perform simultaneously as a sealing element to seal the displacement chamber from case pressure. This double function is especially difficult to solve in those piston machines, which operate in a wide range of temperatures and a large range of operating conditions.

Since Ramelli's first axial piston pump designed in the 17th century, many researchers had worked on piston/cylinder interface. Gerber (1968) presented the first gap flow model for the piston/cylinder interface without consideration of hydrodynamic pressure built up. This effect was later considered by Van der Kolk (1972). The first published measurements of the piston friction forces by Renius (1974) could demonstrate the influence of several geometrical parameters on the load carrying hydrodynamic fluid film. One of his recommendations was a piston-cylinder clearance of 0.1% for usual pumps and motor speeds and little less for low speed applications. He could for example also demonstrate that a barrel like piston profile supports hydrodynamic oil films considerably. His temperature measurements of the oil film confirmed the nature of the friction forces with a lower dissipation for motor than for pump mode. After that, more and more physical phenomena were added into the later piston/cylinder interface models, i.e. piston motion was considered by Yamaguchi (1976), the impact of change of viscosity due to pressure and temperature was considered by Ivantysynova (1983, 1985), Olems (2001) solved the piston force balance considering piston micron motion, Ivantysynova and Huang (2002) added elasto-hydrodynamic effect into consideration by using influence matrix approach.

The authors' research team has developed a fully coupled fluid-structure thermal and multi-body dynamics simulation model (FSTI) for the piston cylinder interface, which was first time published by Pelosi and Ivantysynova (2009). The model not only considers elastic deformation of the piston and cylinder due to

CONTACT Lizhi Shang shangl@purdue.edu

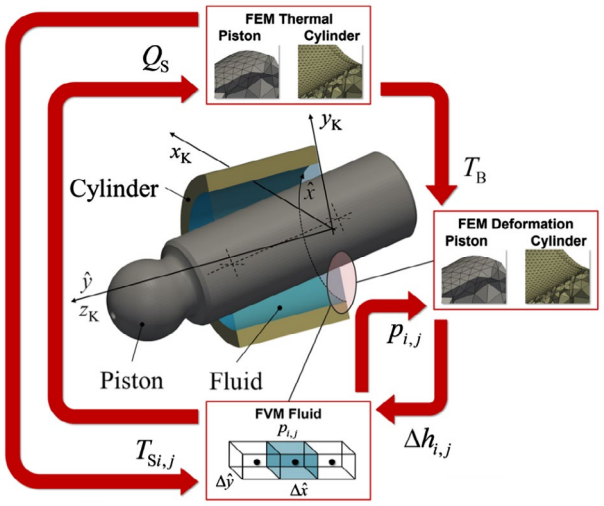

Figure 1. Piston/cylinder lubrication model.

pressure load but also considers thermal expansion due to energy dissipation in the fluid film. The proposed algorithm includes a complete heat transfer model of the cylinder block and piston assembly. Figure 1 illustrates the numerical coupling of different physical domains considered in this novel piston cylinder model. More details about the model and its experimental verification can be found in Pelosi and Ivantysynova (2012a, 2012b, 2013) andin Pelosi (2012).

Along with the development of the simulation approach, many new designs were studied by the researchers. Yamaguchi (1976) proposed a tapered piston shape to improve the hydrodynamic pressure build up according to his modeling study, Ivantysynova (1983) investigated the favorable barrel like piston shape more in depth as first recommended by Renius (1974). The positive influences on the performance have been confirmed also by Lasaar (2003). Ivantysynova and Lasaar (2004) concluded in their paper that energy dissipation reduction can be achieved by using barrel-like piston with reduced clearance.

More contributions of researchers and engineers on piston/cylinder interface design can be found in Ivantysynova (2012). Most of these publications are addressing modelling of conditions with fully generated hydrodynamic oil films.

In this presented research study, the FSTI model together with a recently developed port and case temperature prediction model (Shang and Ivantysynova, 2015) are used to first analyze a piston/cylinder interface design and to predict resulting part temperatures, deformations, the fluid film properties and resulting energy dissipation, friction and leakage dependent on operating temperatures. Based on this analysis the authors propose a novel piston design, which helps to keep the fluid film thickness close to optimal in a large range of operating temperatures. The key idea of the proposed novel piston/cylinder design is the utilization of the thermal deformation of the piston and cylinder.

2. The piston/cylinder interface

The piston in swash plate type axial piston machines conducts a very complex periodical motion, which can be divided in two parts: the piston macro motion and the piston micro motion. The piston macro motion can be derived analyzing the piston kinematics.

Figure 2 shows the basic kinematic relationship for swash plate type machines. The piston displacement s_K is dependent on pitch radius, swash plate angle and angular position of the block.

$$s_K = -R_b \cdot \tan\beta \cdot (1 - \cos\varphi) \tag{1}$$

The piston stroke H_K, which represents the displacement of the piston from outer dead center (ODC) to inner dead center (IDC) yields:

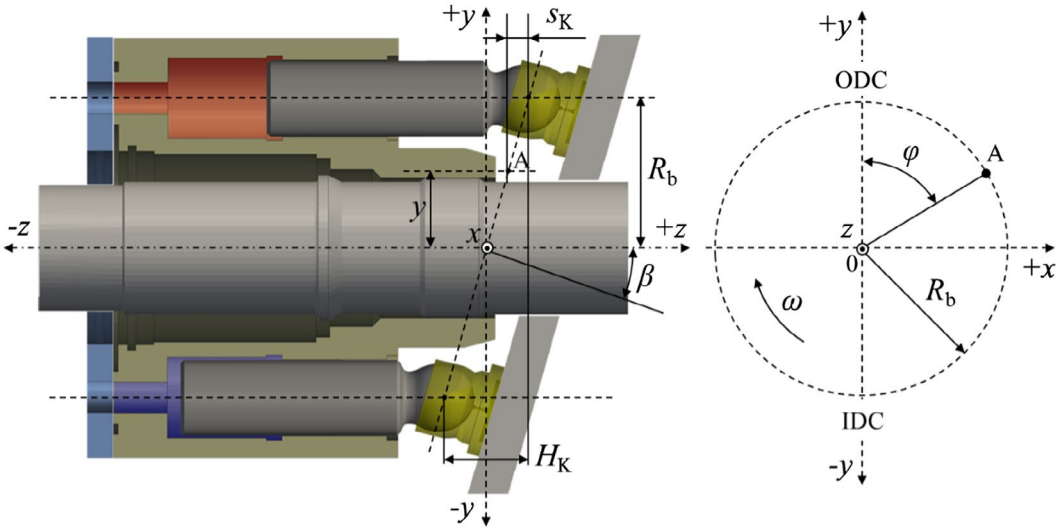

Figure 2. Swash plate type axial piston pump kinematics.

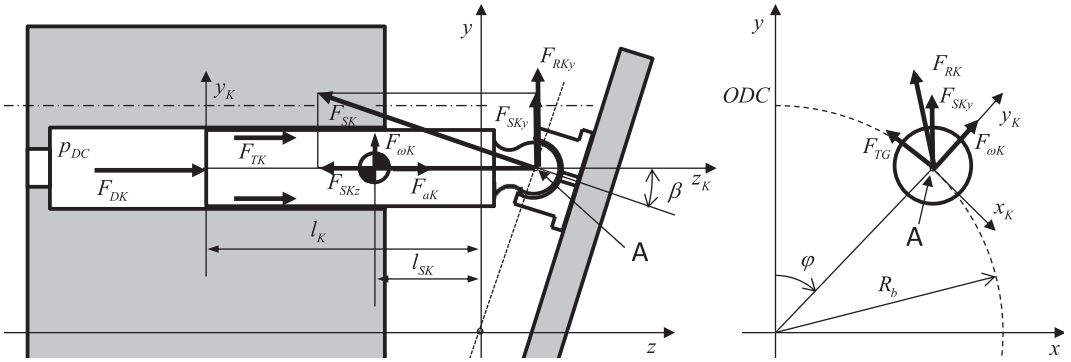

Figure 3. Free body diagram of piston.

$$H_K = 2 \cdot R_b \cdot \tan\beta \tag{2}$$

The axial piston sliding velocity and acceleration are a function of the angular position and angular velocity of the shaft. This axial piston motion represents a forced motion. Besides that, the piston has the freedom to turn about its own axis. The piston turning/spinning motion is not forced and therefore depends on the friction between cylinder and piston and between piston and slipper. Renius (1974) accomplished a very comprehensive experimental study and confirmed the piston spin motion in swash plate type axial piston machines through measurements of piston friction forces in axial and circumferential direction. Later Lasaar (2003) confirmed with his piston friction force measurements using a specially designed swash plate type machine that the piston spin motion is present and its value depends on operating conditions. In addition to the described axial motion and rotation about its axis the piston is conducting a complex micro motion within the cylinder bore. The micro motion can be derived from the force balance of the piston.

2.1. Piston/cylinder interface loading condition

Figure 3 shows a free body diagram of the piston. When the pump or motor runs under pressure the largest force is usually the pressure force F_{DK}. The pressure force is determined by the instantaneous cylinder pressure p_{DC} and therefore changes periodically over one shaft revolution. Similar the piston inertia force F_{aK} changes periodically with the piston acceleration. De-pendent on the fluid film conditions and the resulting flow between piston and cylinder the piston friction force F_{TK} will also act on the piston. Finally, the reaction force of the swash plate F_{SK} and the piston centrifugal force $F_{\omega K}$ will act on the piston. As shown in Figure 3 the component F_{SKy} of swash plate reaction force represents a radial force acting on the piston. In addition the y-components of the piston centrifugal force and the slipper friction force F_{TG} will contribute to the resulting side load of the piston. The resultant force F_{RK}, which acts on the piston perpendicular to the piston axis at point A of the ball joint must be compensated by the fluid film to prevent a rigid contact and wearing between piston and cylinder, i.e. resulting pressure force and moment generated from the fluid film pressure field.

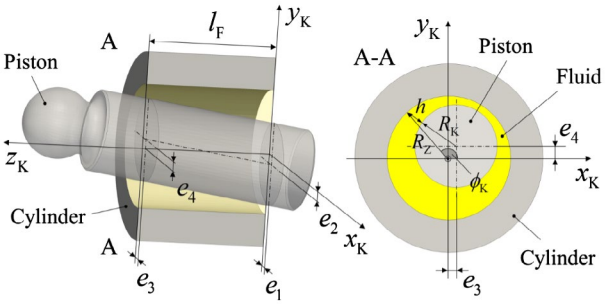

Figure 4. Inclined position of piston in cylinder bore forming the fluid film.

2.2. Piston cylinder interface gap height

The periodically oscillating external forces lead to a complex micro motion of the piston, where the piston changes its inclination angle in the cylinder bore till the resulting hydrodynamic pressure field generates the required resulting fluid force and moments to balance the external forces. Figure 4 shows the resulting inclined piston position of the piston in the cylinder bore at a given angular position of the shaft.

Figure 5 shows an unwrapped fluid film between piston and cylinder at a shaft angle of 135° when the unit is operating at the maximum speed, the maximum pressure and the maximum swash plate angle. The gap height shown in this figure is normalized to its original clearance, however the deformation of surface due to pressure and thermal loading influences the resulting film thickness. That is the reason why the maximum film thickness shown in Figure 5 can be larger than the clearance. The resulting film thickness can be described as a sum of the film thickness resulting from the given clearance and position of the piston inside the bore, the total deformation of piston and cylinder Δh_{def_p} due to pressure and the total deformation of piston and cylinder Δh_{def_th} due to thermal loading:

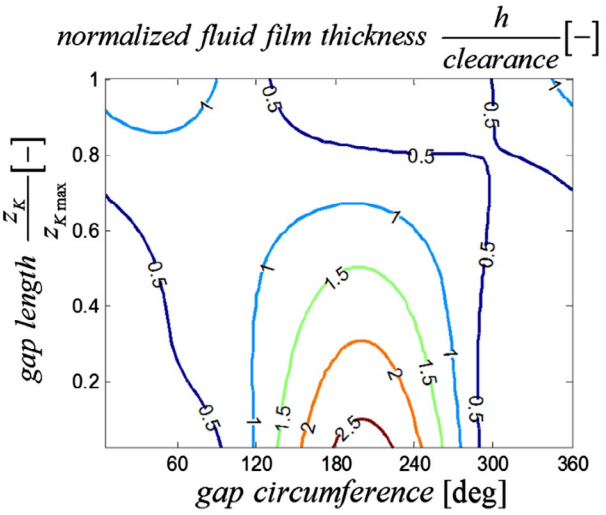

Figure 5. Film thickness for the unwrapped gap without pressure and thermal deformations.

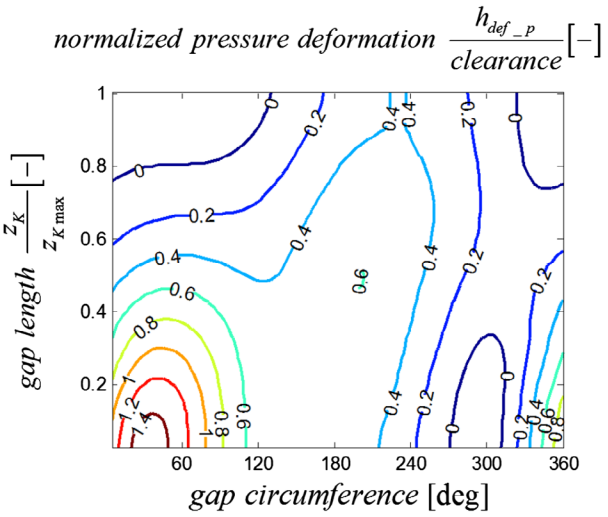

Figure 6. The resulting change of film thickness $\Delta h_{\text{def\_p}}$ due to pressure deformation.

$$h = h_{\text{rigid}} + \Delta h_{\text{def\_p}} + \Delta h_{\text{def\_th}} \tag{3}$$

The total deformations of piston and cylinder $\Delta h_{\text{def\_p}}$ due to pressure deformation and the total deformation of piston and cylinder $\Delta h_{\text{def\_th}}$ due to thermal loading are calculated using Equation 4. The sign convention in Equation 4 is based on the following definition: Positive values of the pressure deformation of the piston $\Delta h_{\text{def\_p\_K}}$, the pressure deformation of the cylinder bore $\Delta h_{\text{def\_p\_B}}$ and the thermal deformation of the cylinder bore $\Delta h_{\text{def\_th\_B}}$ increase film thickness of the interface, while a positive value of the thermal deformation of the piston $\Delta h_{\text{def\_p\_K}}$ reduces the resulting film thickness.

$$\begin{aligned} \Delta h_{\text{def\_p}} &= \Delta h_{\text{def\_p\_K}} + \Delta h_{\text{def\_p\_B}} \\ \Delta h_{\text{def\_th}} &= -\Delta h_{\text{def\_th\_K}} + \Delta h_{\text{def\_th\_B}} \end{aligned} \tag{4}$$

Figure 6 shows the resulting change of film thickness $\Delta h_{\text{def\_p}}$ due to pressure deformation of both piston and cylinder normalized to the original clearance.

In Figure 7 the resulting change in film thickness due to thermal deformation of piston and cylinder $\Delta h_{\text{def\_th}}$ is plotted. Again the values of resulting thermal deformation are normalized to the original clearance.

Figures 5–7 indicate that the parts deformation from both the pressure and thermal load has a big impact on the resulting fluid film thickness. A good understanding of the deformation of solid parts and its impact on the fluid film behavior is needed. A simulation tool that is used to investigate the fluid structure and thermal interaction phenomena is described in the following chapter.

3. Simulation methodology

The total energy dissipation generated in the viscous fluid in the gap between the piston and the cylinder bore can be described as:

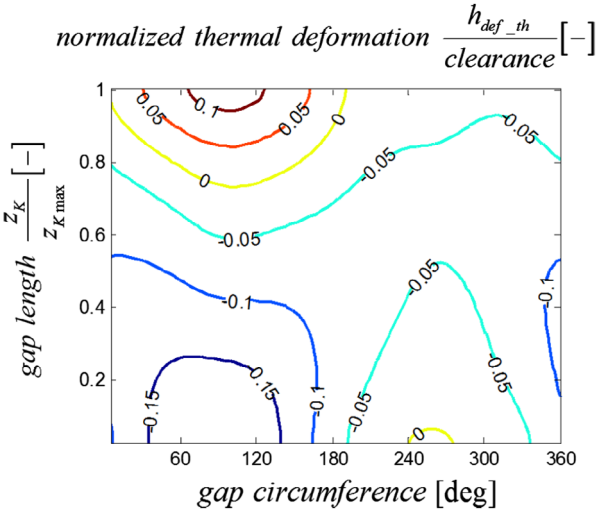

Figure 7. The resulting change of film thickness $\Delta h_{\text{def\_th}}$ due to thermal deformation.

$$\Phi = \int_V \mu \left[\left(\frac{\partial v_x}{\partial z} \right)^2 + \left(\frac{\partial v_y}{\partial z} \right)^2 \right] \cdot dV \tag{5}$$

where x and y are circumferential and axial direction of the fluid film, and z is the direction of the fluid film thickness.

The FSTI model calculates the total energy dissipation of the piston/cylinder interface based on the Equation (5). To solve this simple equation, the viscosity, velocity, pressure and temperature of the fluid in a three dimensional space must be solved. Therefore, the piston position, the piston micro motion, the deformation of the piston and cylinder due to pressure and thermal loading and the heat transfer for the piston/cylinder interface need to be solved as well. The port and case flow temperature model calculates the outlet and case

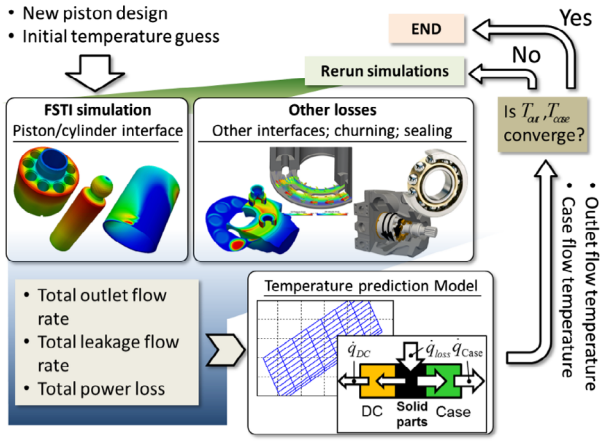

Figure 8. The flow chart of the simulation methodology.

flow temperatures. The FSTI model utilizes the port and case flow temperatures as boundary conditions to solve the three dimensional heat transfer of the parts. These important temperatures highly depend on the power loss and the leakage of the total unit, therefore, will change with the piston design.

The total power loss of the unit is generated by the energy dissipation of piston/cylinder interface the energy dissipation of the slipper/swash plate interface, the energy dissipation of the cylinder block/valve plate interface, the power loss due to the churning motion of the rotation group, and the friction in seal and bearing components. To study different piston designs, only the change of energy dissipation caused by the piston design is considered, i.e. all other power losses are assumed to remain constant.

Similarly, the total leakage flow of the total unit is generated by the leakage flow in piston/cylinder interface and the leakage flow in the slipper/swash plate interface and the cylinder block/valve plate interface. To study different piston designs, the leakage flow from the piston/cylinder will change while leakage from the other two interfaces are assumed to remain constant.

Figure 8 shows the flow chart explaining the simulation methodology for this research study on piston design. A new piston design will be simulated with an initial temperature guess in order to start the iteration, then the calculated energy dissipation and leakage flow rate of piston/cylinder interface will be used together with the unchanged remaining power losses of the unit to calculate the total power loss. Same method is used to calculate the total leakage of the unit while varying the piston design. The resulting total power loss and leakage will be fed into the temperature prediction model, then, the outlet flow temperature and case flow temperature can be calculated and be used as temperature boundaries for the FSTI simulation in the next iteration. This iterative loop will continue until the temperatures converge and the resulting performance of the new piston design can be obtained.

4. Baseline clearance design

Clearance, which is defined as the diameter difference between the cylinder bore and the piston, is a very important design parameter. A high clearance will result in high leakage loss and a low clearance will result in high friction loss. An analytical method to find optimal clearance, which was published by Ivantysyn and Ivantysynova (1993), assuming parallel gap between piston and cylinder bore was used to determine the baseline clearance.

The power loss due to leakage can be derived as:

$$P_{SQ} = Q_{SL} \cdot \Delta p \tag{6}$$

where the leakage flow rate Q_{SL} can be calculated assuming parallel gap:

$$Q_{SL} = \frac{\pi \cdot d_K \cdot h^3}{12 \cdot \mu \cdot l_K} \cdot \Delta p \tag{7}$$

The power loss due to friction assuming parallel gap applies:

$$P_{ST} = F_{TK} \cdot v_K = \mu \cdot \frac{v_K^2}{h} \cdot \pi \cdot d_K \cdot l_K \tag{8}$$

The total power loss in the piston/cylinder interface assembly is then:

$$P_S = \frac{\pi \cdot d_K \cdot h^3}{12 \cdot \mu \cdot l_K} \cdot \Delta p^2 + \mu \cdot \frac{v_K^2}{h} \cdot \pi \cdot d_K \cdot l_K \tag{9}$$

The optimal gap height occurs when $\frac{dP_S}{dh} = 0$ and yields:

$$h_{opt} = 1.414 \cdot \sqrt{\mu \cdot l_K \cdot \frac{v_K}{\Delta p}} \tag{10}$$

By applying the fluid viscosity at 52 °C, which is the normal operating temperature, the stock unit geometry, the operating pressure of 400 bar, and the piston velocity calculated from the unit geometry and the maximum operating speed, an optimal gap height of 0.055% of the piston diameter can be solved. The optimal clearance is twice of the optimal gap height, which is 0.11% of the piston diameter.

This clearance is theoretically calculated based on a constant fluid viscosity, however, the fluid viscosity varies with the fluid temperature and pressure. From Roelands (1966) the viscosity-temperature-pressure relationship can be described as:

$$\log \mu + 1.2 = G_0 \cdot \frac{\left(1 + \frac{p}{2000}\right)^z}{\left(1 + \frac{T}{135}\right)^s} \tag{11}$$

In Equation (11), only three parameters, G_0, Z, and S suffice for defining the complete viscosity-temperature-pressure relationship of a given fluid. The authors

Table 1. Calculated kinematic viscosity at different temperature and pressure.

Fluid kinematic viscosity (cSt)			
	120 [°C]	60 [°C]	−20 [°C]
1[bar]	4.6	16.6	803.3
400[bar]	7.3	30.7	2374.8

Table 2. Three different operating temperatures.

*T*_in [°C]	100	52	−20
*T*_out [°C]	106	58	−14
*T*_case [°C]	121	77	34

Table 3. Normalized simulated energy dissipation.

	*T*_in = 100 °C	*T*_in = 52 °C	*T*_in = −20 °C
Half speed	1.33%	1.30%	5.57%
Full speed	1.29%	1.66%	7.54%

used given measured viscosity values of HLP 32 fluid at different temperature and pressure to calculate these three parameters and use these them to calculate the fluid's kinematic viscosity.

Table 1 shows an example of the variation on calculated kinematic viscosity with pressure and temperature (the kinematic viscosity is calculated from the dynamic friction from Equation (11) and the density changes with pressure and temperature). The numbers show that the fluid viscosity increases over 300 times with the decreasing temperature.

5. Simulation study of baseline design at different operating temperatures

Steel and Brass as a tribological material pair are commonly used for the piston/cylinder interface. Steel is used for piston and brass is used for cylinder block or bushing. These two materials cannot be used oppositely because the maximum stress of the piston (most likely the piston neck) is normally higher than 1000 MPa which is much higher than the yield strength of brass.

The authors keep the stock unit material combination, which are steel piston, steel cylinder block and brass bushing, and set the piston/cylinder clearance to 0.11% of the piston diameter according to the calculation from previous chapter. Three inlet flow temperatures were chosen which are shown in the first row of Table 2. The in house port and case flow temperature prediction model was used to calculate the outlet flow temperatures and case flow temperatures. Those temperatures are shown in the second row and the third row of Table 2. Besides of three sets of operating temperatures, the authors also chose two different speeds: the maximum speed of the stock unit and the half speed of the stock unit. Therefore, this baseline design is simulated at six different operating conditions.

Table 3 shows the simulated energy dissipation in all the piston/cylinder interfaces normalized to the theoretical output power of the total unit.

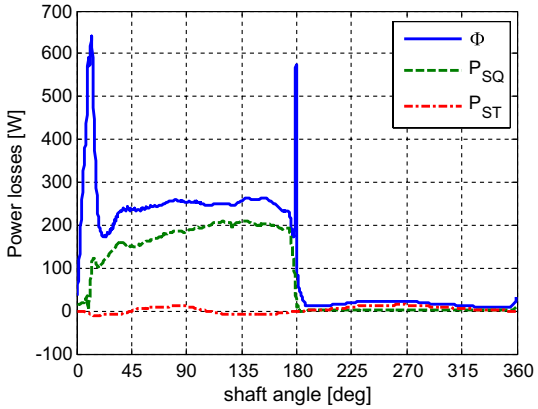

Figure 9. Total energy dissipation, power loss due to leakage, and power loss due to friction @ 100 °C half speed.

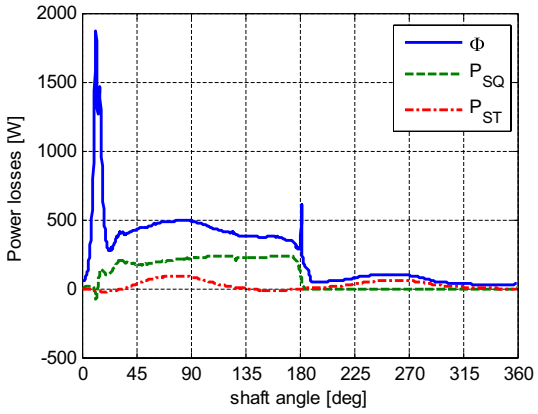

Figure 10. Total energy dissipation, power loss due to leakage, and power loss due to friction @ 100 °C full speed.

The energy dissipations were calculated from Equation (5). The total power loss defined in Equation (9) is only valid for parallel gap and is underestimated since the other parts of power loss such as the friction of spinning motion of the piston, and the micro squeezing motion are missing.

However, by applying the simulated leakage flow rate and the axial friction force into Equation (6) and Equation (8), the power loss due to leakage and the power loss due to the axial friction can be calculated. Even though these two power losses do not cover all the power losses in the gap, the comparison of these two can be helpful toward the full understanding of the fluid film behavior.

By substituting the optimal gap height from Equation 10 into the power loss due to the leakage from equation 6 and the power loss due to the friction from Equation 8, an optimal ratio between the power loss due to friction and power loss due to leakage yields:

$$r_P = \frac{P_{ST}}{P_{SQ}} = 3 \tag{12}$$

Figure 9 through Figure 14 show the total energy dissipation Φ, the power loss due to leakage P_{SQ} and the

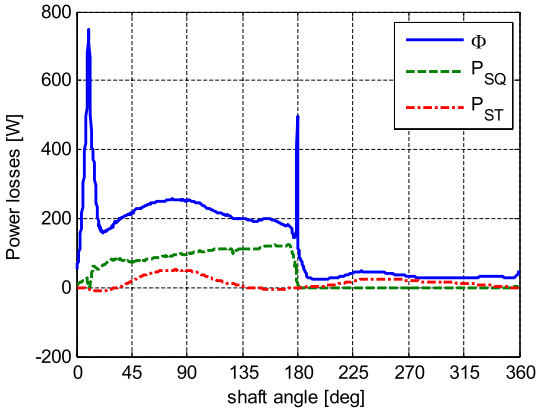

Figure 11. Total energy dissipation, power loss due to leakage, and power loss due to friction @ 52 °C half speed.

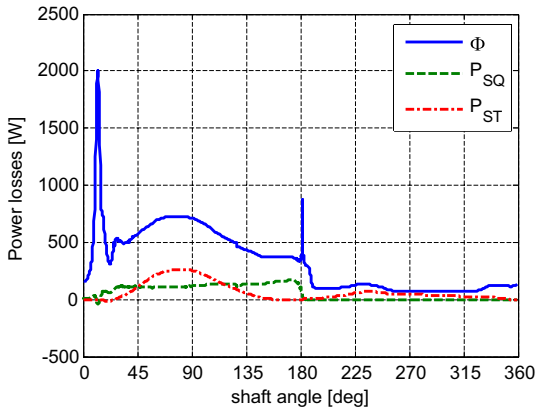

Figure 12. Total energy dissipation, power loss due to leakage, and power loss due to friction @ 52 °C full speed.

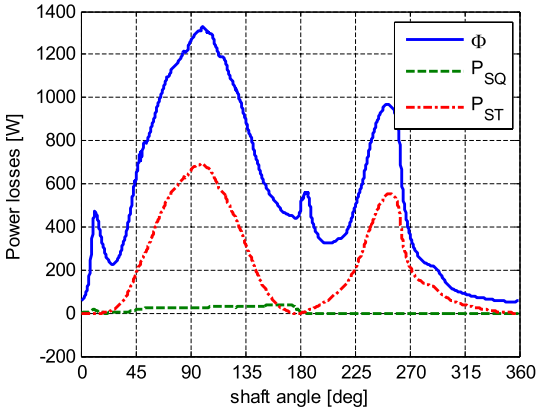

Figure 13. Total energy dissipation, power loss due to leakage, and power loss due to friction @ −20 °C half speed.

power loss due to the axial friction P_{ST} for a single piston/cylinder interface for the six operating conditions. The energy dissipation spikes around 0 and 180° are due to the rapid pressure change in the displacement chamber and the associate parts deformation and the squeezing motions. These figures show that at high temperature the power loss due to leakage dominates whereas at low temperature the power loss due to friction dominates.

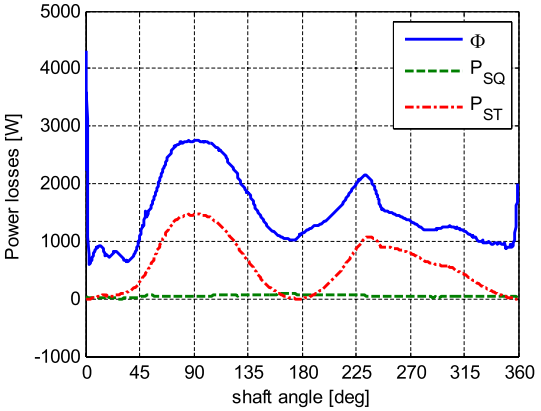

Figure 14. Total energy dissipation, power loss due to leakage, and power loss due to friction @ −20 °C full speed.

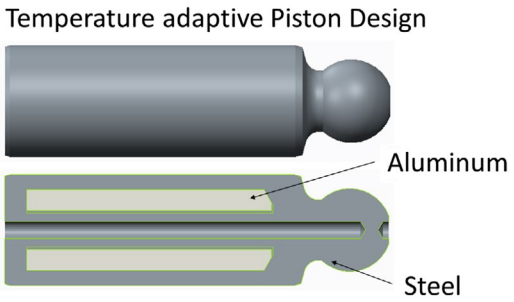

Figure 15. Temperature adaptive piston design.

The simulation results of the baseline design indicate that the optimal clearance for the high temperature operating condition is lower in order to seal the less viscous fluid better. And, for the low temperature operating condition, the optimal clearance is higher in order to reduce the friction. However, since the clearance of the baseline unit is designed for 52 °C, the gap height at other temperatures is far away from the optimum.

6. Temperature adaptive piston design concept

The authors investigated a novel piston design to use thermal deformation of the piston and cylinder in order to keep the resulting film thickness closer to the optimum in a wide range of operating temperatures.

A material with higher thermal expansion coefficient like bronze, brass, or aluminum can be used to allow the piston to deform more under the thermal load than the steel baseline piston. However the piston design must be able to withstand the maximum stress of the piston neck, which is normally much higher than the yield strength of any of those materials.

Therefore the authors propose a bi-metal piston design as shown in Figure 15. Comparing to the baseline piston design as shown in Figure 16, the proposed piston design uses the same high yield strength of steel to bear the stress, and uses the high thermal expansion

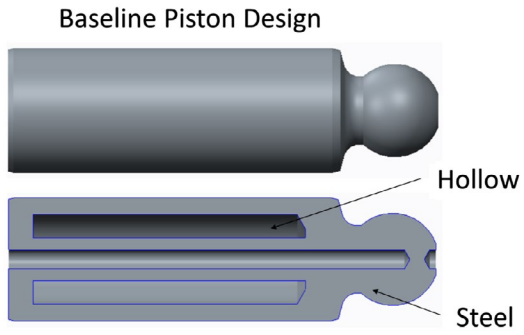

Figure 16. Baseline piston design.

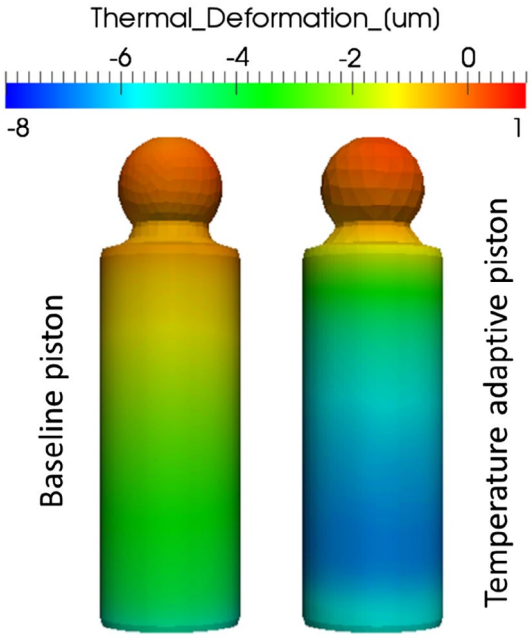

Figure 17. Thermal deformation comparison when operate with −20 °C inlet flow.

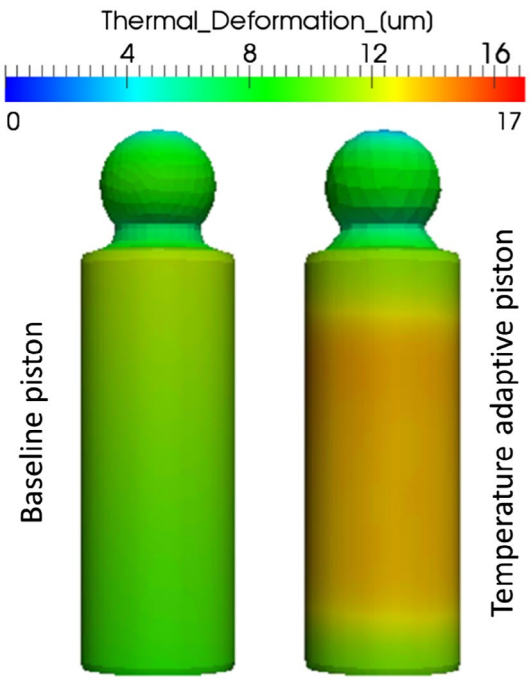

Figure 18. Thermal deformation comparison when operate with 100 °C inlet flow.

Table 4. Normalized Δh_{def_th} for baseline piston design.

	T_in = 100 °C	T_in = 52 °C	T_in = −20 °C
Half speed	−8.20%	−9.27%	−4.54%
Full speed	−8.98%	−7.65%	−3.76%

Table 5. Normalized Δh_{def_th} for temperature adaptive piston design.

	T_in = 100 °C	T_in = 52 °C	T_in = −20 °C
Half speed	−22.84%	−9.78%	11.32%
Full speed	−21.03%	−7.15%	15.28%

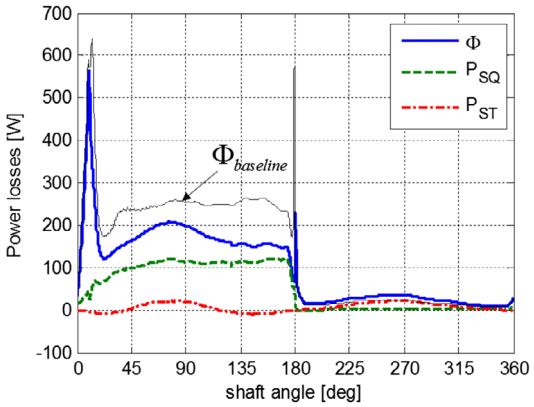

Figure 19. Total energy dissipation, power loss due to leakage, and power loss due to friction @ 100 °C half speed.

coefficient of another material like aluminum to adapt the film thickness to the changing operating temperature.

7. Simulation result for the temperature adaptive piston

In this chapter, the temperature adaptive piston simulation results will be presented and compared to the baseline piston design.

Firstly, Figures 17 and 18 show how both the baseline piston and the temperature adaptive piston deform under thermal load. Figure 17 shows the thermal deformation comparison between the baseline piston and the temperature adaptive piston when operating at −20 °C inlet flow temperature. This figure shows that the temperature adaptive piston shrinks 6 microns more than the baseline piston at low temperature operating condition.

Figure 18 shows the deformation comparison between the baseline piston and the temperature adaptive piston when operating at 100 °C inlet flow temperature. This figure shows that the temperature adaptive piston expands 4 microns more than the baseline piston at high temperature operating conditions.

Table 4 shows the normalized total thermal deformation of piston and cylinder Δh_{def_th} of baseline piston design, this deformation is normalized to the clearance. The normalized Δh_{def_th} does not show big variation over

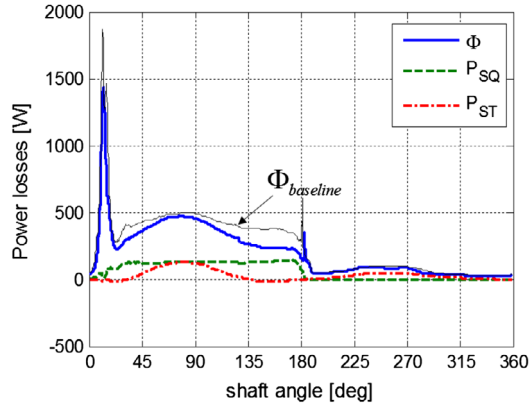

Figure 20. Total energy dissipation, power loss due to leakage, and power loss due to friction @ 100 °C full speed.

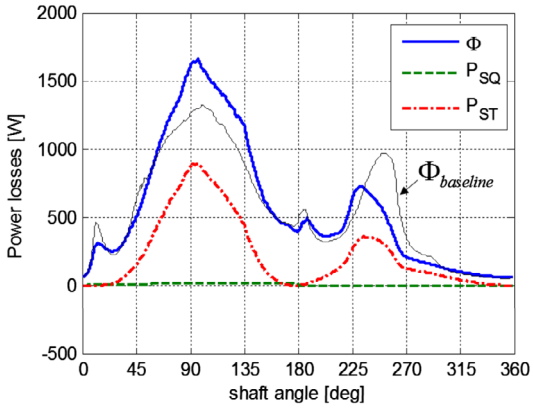

Figure 23. Total energy dissipation, power loss due to leakage, and power loss due to friction @ −20 °C half speed.

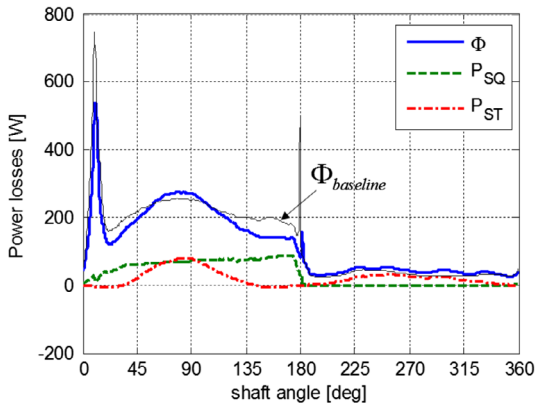

Figure 21. Total energy dissipation, power loss due to leakage, and power loss due to friction @ 52 °C half speed.

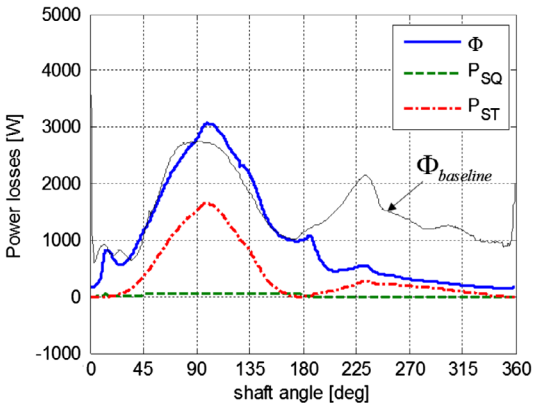

Figure 24. Total energy dissipation, power loss due to leakage, and power loss due to friction @ −20 °C full speed.

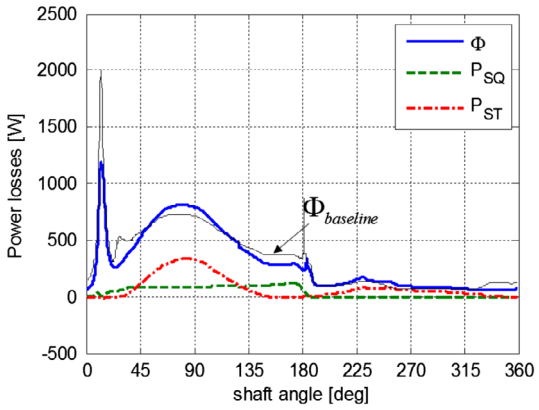

Figure 22. Total energy dissipation, power loss due to leakage, and power loss due to friction @ 52 °C full speed.

all six operating conditions. Table 5 shows the normalized $\Delta h_{\text{def\_th}}$ of temperature adaptive piston design and the maximum of 38% difference can be found in this case. The comparison of Tables 4 and 5 shows that the temperature adaptive piston reduces the gap height at high temperature operating condition and increases the gap height at low temperature operating condition.

Table 6. Comparing the t.a.p. energy dissipation to the energy dissipation of the baseline piston design.

	$T\_in = 100$ °C	$T\_in = 52$ °C	$T\_in = -20$ °C
Half speed	74.23%	91.44%	102.37%
Full speed	80.25%	91.93%	68.02%

Figure 19 through Figure 24 show the total energy dissipation Φ, the power loss due to leakage P_{SQ} and the power loss due to the axial friction P_{ST} of the temperature adaptive piston design for all nine piston/cylinder interfaces for the six operating conditions.

The simulation study shows that performance of the piston/cylinder interface took the advantage of the thermal deformation of the temperature adaptive piston. Table 6 shows the energy dissipation of temperature adaptive piston (t.a.p.) simulation result normalized by the baseline energy dissipation. This table shows that the temperature adaptive piston reduces the energy dissipation more than 20% at 100 °C and reduce more than 30% at −20 °C full speed, and slight increase the energy dissipation at −20 °C half speed. This comparison results show that the proposed temperature adaptive piston has an overall better performance than the baseline piston design.

8. Conclusion

In this paper, a novel piston design is proposed to reduce the energy dissipation of the piston/cylinder interface by utilizing the thermal deformation at different temperatures. The simulation approach is presented in this paper as well as the simulation results. The simulation results show overall improvement of the interface performance by comparing the proposed piston design to the baseline.

It has been demonstrated, that the novel temperature adaptive piston design is able to reduce the energy dissipation of the piston cylinder interface in a wide range of operating temperatures.

Nomenclature

d_K	Piston diameter [m]
H_K	Piston stroke [m]
F_{DK}	Pressure force on piston [N]
F_{aK}	Axial piston inertia force [N]
F_{TK}	Piston/cylinder friction force [N]
F_{SK}	Reaction force [N]
F_{SKz}	Reaction force in z direction [N]
F_{SKy}	Reaction force in y direction [N]
$F_{\omega K}$	Radial piston inertia force [N]
F_{TG}	Slipper/swashplate friction [N]
F_{RK}	Resulting side load of piston [N]
F_{RKy}	Resulting side load of piston in y direction [N]
F_{ST}	Piston/cylinder friction [N]
G_o	Coefficient to calculated fluid viscosity [–]
h	Gap height [m]
h_{rigid}	Gap height without deformation [m]
h_{opt}	Optimal gap height [m]
l_K	Piston gap length [m]
p	Pressure [bar]
p_{DC}	Displacement chamber pressure [bar]
P_{SQ}	Power loss due to leakage [W]
P_{ST}	Power loss due to friction [W]
P_S	Total power loss [W]
Q_{SL}	Leakage flow rate [m³/s]
r_p	Power loss ratio [–]
R_b	Pitch radius [m]
s	Coefficient to calculated fluid viscosity [–]
s_K	Piston displacement [m]
T	Temperature [°C]
T_{in}	Inlet flow temperature [°C]
T_{out}	Outlet flow temperature [°C]
T_{case}	Case flow temperature [°C]
V	Volume [m³]
v_K	Piston velocity [m/s]
z	Coefficient to calculated fluid viscosity [–]
β	Swash plate angle [rad]
Δh_{def_p}	Total pressure deformation [m]
Δh_{def_th}	Total thermal deformation [m]
$\Delta h_{def\_p\_K}$	Pressure deformation of piston [m]
$\Delta h_{def\_p\_B}$	Pressure deformation of cylinder bore [m]
$\Delta h_{def\_th\_K}$	Thermal deformation of piston [m]
$\Delta h_{def\_th\_B}$	Thermal deformation of cylinder bore [m]
Δp	Pressure difference through gap [Pa]
Φ	Energy dissipation [W]
φ	Shaft angle [rad]
μ	Fluid dynamic viscosity [Pa s]

Disclosure statement

No potential conflict of interest was reported by the authors.

Notes on contributors

Lizhi Shang Born on 25 March 1989 in Tianjin (China). He received his B.S. degree in Thermal Energy and Power Engineering from Huazhong University of Science and Technology in 2011 and his M.S. degree in Mechanical Engineering in New Jersey Institute of Technology in 2013. He is currently a PhD student at Maha Fluid Power Research Center in Purdue University. His main research interests are modeling and optimizing of hydraulic pumps/motors.

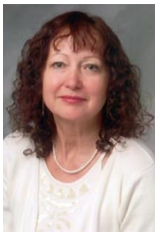

Monika Ivantysynova Born on 11 December 1955 in Polenz (Germany). She received her MSc. Degree in Mechanical Engineering and her PhD. Degree in Fluid Power from the Slovak Technical University of Bratislava, Czechoslovakia. After 7 years in fluid power industry she returned to university. In April 1996 she received a Professorship in fluid power & control at the University of Duisburg (Germany). From 1999 until August 2004 she was Professor of Mechatronic Systems at the Technical University of Hamburg-Harburg. Since August 2004 she is Professor at Purdue University, USA. Her main research areas are energy saving actuator technology and model based optimisation of displacement machines as well as modelling, simulation and testing of fluid power systems. Besides the book 'Hydrostatic Pumps and Motors' published in German and English, she has published more than 80 papers in technical journals and at international conferences.

References

Gerber, H. 1968. Les elements de calcus des machines volumetriques a piston axiaux e-t á distribution par glace. Energie Fluide et Lubrification et Hydraulique Pneumatiquee et Asservissements (EFL+HPA) No. 4, pp. 61–67, No. 9, pp. 53–62, No. 11, pp. 53–56

Ivantysyn, J. and Ivantysynova, M., 1993. *Hydrostatische Pumpen und Motoren* [Hydrostatic pumps and motors]. Würzburg: Vogel Buchverlag.

Ivantysynova, M. (at that time Berge, M. 1983. *An investigation of viscous flow in lubricating gaps*. (In Slovak). Dissertation. SVST Bratislava, Czechoslovakia.

Ivantysynova, M., 1985. Temperaturfeld im Schmierspalt zwischen Kolben und Zylinder einer Axialkolbenmaschine [Temperature distribution in lubricating gap between Piston and Cylinder in Axial piston machine]. *Maschinenbautechnik*, 34, 532–535.

Ivantysynova, M., 2012. The piston cylinder assembly in piston machines – a long journey of discovery. *Proceedings of 8th IFK International Conference on Fluid Power*. Dresden, Germany: Keynote Lecture, Vol. 3. pp. 307–332.

Ivantysynova, M. and Huang, Ch. 2002. Investigation of the gap flow in displacement machines considering the elastohydrodynamic effect. *5th JFPS International Symposium on Fluid Power*. Nara, Japan: The Japan Fluid Power System Society. pp. 219–229.

Ivantysynova, M. and Lasaar, R. 2004. An investigation into micro- and macrogeometric design of piston/cylinder assembly of swash plate machines. *International journal of fluid power*, 5 (1), 23–36.

Lasaar, R. 2003. *Eine Untersuchung zur mikro-und makrogeometrischen Gestaltung der Kolben/ Zylinder-baugruppe von Schrägscheibenmaschinen* [An investigation into Micro- and macrogeometric design of piston/cylinder assembly of swash plate machines]. Fortschritt-Berichte VDI Reihe 1 No. 364, Düsseldorf: VDI Verlag Düsseldorf.

Olems, L. 2001. *Ein Beitrag zur Bestimmung des Temperaturverhaltens der Kolben-Zylinder-Baugruppe von Axialkolbenmaschinen in Schrägscheibenbauweise* [A contribution to the determination of the temperature behavior of the piston-cylinder interface of swashplate type axial piston machine]. Fortschritt-Berichte VDI. Reihe 1 No. 348. Düsseldorf: VDI. ISBN: 3-18-334801-2

Pelosi, M. 2012. *An investigation on the fluid-structure interaction of piston/cylinder interface*. Thesis (PhD). Purdue University.

Pelosi, M. and Ivantysynova, M., 2009. A novel thermal model for the piston/cylinder interface of piston machines. *Bath ASME symposium on fluid power and motion control (FPMC2009)*, Bath. [DSCC2009-2782].

Pelosi, M. and Ivantysynova, M., 2012a. A geometric multigrid solver for the piston-cylinder interface of axial piston machines. *Tribology transactions*, 55 (2), 163–174.

Pelosi, M. and Ivantysynova, M., 2012b. Heat transfer and thermal elastic deformation analysis on the piston/cylinder interface of axial piston machines. Transaction of the ASME, journal of tribology, 134 Oct, 1–15.

Pelosi, M. and Ivantysynova, M., 2013. The impact of axial piston machines mechanical parts constraint conditions on the thermo-elastohydrodynamic lubrication analysis of the fluid film interfaces. *International journal of fluid power*, 14 (3), 35–51.

Renius, K.T. 1974. *Untersuchung zur Reibung zwischen Kolben und Zylinder bei Schrägscheiben-Axialkolbenmaschinen* [Investigation of friction between piston and cylinder in swashplate type axial piston machine]. *VDI Forschungsheft 561*. Düsseldorf: VDI Verlag.

Roelands, C.J.A., 1966. *Correlational aspects of the viscosity-temperature-pressure relationship of lubricating oils*. Druk, V. R. B., Groingen.

Shang, L. and Ivantysynova, M., 2015. Port and case flow temperature prediction for axial piston machines. *International Journal of Fluid Power*, 16 (1), 35–51.

Van der Kolk, H.J. 1972. *Beitrag zur Bestimmung der Tragfähigkeit des stark verkanteten Gleitlagers Kolben – Zylinder an Axialkolbenpumpen der Schrägscheibenbauart* [Contribution to the determination of the load carrying capacity of the strongly tilted piston – cylinder sliding bearing in swashplate type axial piston machine]. Dissertation. Uni Karlsruhe.

Yamaguchi, A., 1976. Motion of pistons in piston-type hydraulic machines : 1st. report : theoretical analysis. *Bulletin of JSME*, 19 (130), 402–407.